Influence of long-term creep exposure on the microstructure stability of cast Ti-46Al-2W-0.5Si alloy for turbine blades

J. Lapin[1]* , T. Pelachová[1], M. Dománková[2], D. Daloz[3], M. Nazmy[4]

[1]*Institute of Materials and Machine Mechanics, Slovak Academy of Sciences, Račianska 75, 831 02 Bratislava, Slovak Republic*
[2]*Faculty of Material Sciences and Technology, Slovak Technical University, Paulínska 16, 917 24 Trnava, Slovak Republic*
[3]*Ecole Nationale Supérieure des Mines de Nancy, LSG2M, Parc de Saurupt, F-54042 Nancy, Cedex, France*
[4]*ALSTOM Ltd., Department of Materials Technology, TGTM.D, CH-5401 Baden, Switzerland*

Abstract

The effect of long-term creep exposure on the microstructure stability of a cast TiAl-based alloy with nominal chemical composition Ti-46Al-2W-0.5Si (at.%) was studied. Constant load tensile creep tests were performed at temperature range 973–1123 K and at applied stresses ranging from 138 to 350 MPa up to 25677 h. The creep curves exhibit short primary creep stage that is directly followed by tertiary creep. For the selected long-term creep regimes, the minimum creep rate is measured to vary from 1.93×10^{-9} to 2.83×10^{-10} s^{-1} and depends on the applied stress and temperature. The absence of secondary creep stage is related to stability of initial α_2/γ microstructure and formation of deformation twins. During creep the α_2(Ti$_3$Al) phase in the lamellar and feathery regions transforms partially to the γ(TiAl) phase, needle-like B2 precipitates and occasionally to fine spherical Ti$_5$Si$_3$ silicide particles. Final microstructures of all creep specimens contain four phases $\alpha_2 + \gamma + $ B2 $ + $ Ti$_5$Si$_3$. The applied stresses are shown to accelerate coarsening kinetics of the needle-like B2 precipitates.

1. Introduction

Among various metallic materials for high temperature structural applications in gas turbines and automotive industry such as nickel-based superalloys [1–4], nickel- [5–7] or iron- [8–11] based intermetallic alloys and conventional titanium alloys [12, 13], considerable interest has been devoted to multiphase intermetallic γ-TiAl alloys [14–26]. Low density, high melting temperature, good elevated-temperature strength and modulus retention, high resistance to oxidation, excellent creep properties and competitive properties/cost ratio of cast TiAl-based alloys make them potential candidate structural materials for processing of turbine blades, turbocharger wheels and automotive valves. In recent years a particular interest was devoted to an alloy with nominal chemical composition Ti-46Al-2W-0.5Si (at.%), which was designated as ABB-2 [14, 17, 20]. This alloy belongs to the second generation of TiAl-based alloys developed and patented in nineties of the last century by Nazmy and Staubli [27]. As shown in previous studies [23, 24], large prototype turbine blades can be successfully cast from ABB-2 alloy. However, after thermo-mechanical heat treatments and relaxation annealing the microstructure of turbine blades was not homogenous and changed from fully or nearly lamellar columnar grains in the vicinity of the blade surface to duplex equiaxed grains in the central part. Attempts to homogenize the microstructure of the cast components by increasing annealing temperature or/and annealing time showed undesirable growth of recrystallized equiaxed grains leading to a significant decrease of room-temperature ductility [28]. Altern-

T a b l e 1. Chemical composition of the components from ABB-2 alloy (at.%)

Material	Ti	Al	W	Si	Cu	C	Fe	N	O	H
Bars	Bal	46.61	1.88	0.49	0.006	0.034	0.038	0.057	0.177	0.060
Blade 1	Bal	46.88	1.96	0.53	0.004	0.024	0.041	0.032	0.193	0.040
Blade 2	Bal	46.23	2.00	0.48	0.001	0.017	0.015	0.038	0.087	0.081

T a b l e 2. Test temperature, applied stress, time to 1 % creep deformation, minimum creep rate, deformation to fracture and creep time for the studied creep specimens

Specimen	Temperature (K)	Applied stress (MPa)	Time to 1 % deformation (h)	Minimum creep rate (s^{-1})	Deformation to fracture (%)	Creep time (h)
3B2	1023	200	8100	2.83×10^{-10}	6.7	25677
2A2	973	350	2144	9.58×10^{-10}	6.4	7495
2C3	1033	138	4100	7.63×10^{-10}	14.8	14600
3A2	1123	150	596	1.93×10^{-9}	12.1	3140

ative method for microstructure homogenization and grain refinement using γ massive transformations during quenching from solution annealing temperature or by cyclic heat treatments [18] can lead to severe distortion or even to cracking of the blades due to high cooling rates required for this purpose (water or oil quenching). Hence it is necessary to accept microstructural and mechanical property gradients within the cast complex shaped components from the ABB--2 alloy. Although several studies were published on the microstructure of the ABB-2 alloy [24, 26, 29, 30], information about long-term microstructural stability of large cast components during creep testing are still lacking. Therefore, evaluation of long-term microstructural stability of samples prepared from different regions of cast turbine blades from ABB-2 alloy is of great industrial interest to get reliable experimental data, which can be compared to those of nickel-based superalloys currently used for blades in low pressure stage of stationary gas turbines.

The aim of this paper is to investigate the effect of long-term creep exposure on the microstructure stability of a cast intermetallic Ti-46Al-2W-0.5Si (at.%) alloy, which was developed for turbine blades and turbocharger wheels. It should be noted that the results of the creep tests of shorter duration up to about 7700 h for the ABB-2 alloy have been already published in our previous works [20, 22]. The originality of this work is in exceptionally long duration of creep experiment (up to about 25677 h) comparing to existing literature data that have been published for the emerging class of TiAl-based alloys. From the industrial point of view, these long-term experiments with specimens prepared from industrially cast prototype blades are more relevant for evaluation of a real potential of a specific alloy than the tests of simple ingots prepared in laboratory conditions.

2. Experimental procedure

Creep experiments were conducted on ABB-2 specimens prepared from cast plate with a thickness of 22 mm roughly corresponding to a root part thickness of turbine blades and two large turbine blades with a length of about 600 mm and root part width of 160 mm with the chemical composition given in Table 1. The as-received components were subjected to a hot isostatic pressing at 1533 K under a pressure of 172 MPa for 4 h, which was followed by solution annealing at 1623 K for 1 h and gas fan cooling. The heat treatment was accomplished by relaxation annealing at 1273 K for 6 h and furnace cooling to room temperature.

Cylindrical creep specimens with gauge diameters of 7 and 10 mm were cut from all three cast components by electro spark machining. The longitudinal axis of the creep specimens was parallel to the longitudinal axis of the components. Constant load tensile creep tests were performed at applied stresses ranging from 138 to 350 MPa and at temperature range 973–1123 K up to 25677 h in air. The creep conditions for each evaluated specimen are listed in Table 2. The test temperature was monitored with two thermocouples touching the specimen gauge section and held constant within ± 1 K for each individual test. The specimen displacement was measured using a high-temperature extensometer attached to the ledges of the creep specimen. The acquisition of time-elongation data was accomplished by a computer.

The microstructure analysis was performed by light optical microscopy (LOM), scanning electron microscopy (SEM), transmission electron microscopy (TEM), and energy-dispersive X-ray spectroscopy. LOM and SEM samples were prepared using standard metallographic techniques and etched in a reagent
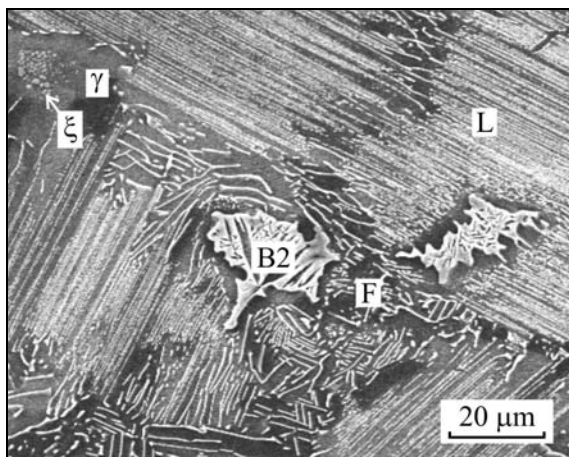
Fig. 1. SEM micrograph showing the typical microstructure of the ABB-2 alloy before creep testing. L – lamellar region, F – feathery region, ξ – Ti_5Si_3 particles, γ – TiAl rich region.

Fig. 2. Dependence of creep strain on the time. The creep temperatures and applied stresses are indicated in the figure.

of 50 ml H_2O, 3 ml HNO_3 and 1.5 ml HF. TEM samples were thinned mechanically to a thickness of about 4 μm and then by ion milling until perforation. TEM analysis was conducted using JEOL 500 microscope operating at 200 kV. The coexisting phases were identified from selected area diffraction patterns using TEM. The interlamellar spacing, size of precipitates and volume fraction of coexisting microstructure regions were determined by computerized image analysis. For this purpose, statistical number of digitalized LOM and SEM micrographs (20 to 30 photos) was taken for each creep regime.

3. Results

3.1. Microstructure before creep testing

Figure 1 shows the typical microstructure of the specimens before creep testing. Quantitative metallography measurements revealed that the microstructure contains (66 ± 3) vol.% of lamellar, (26 ± 3) vol.% of feathery and (8 ± 2) vol.% of γ-rich regions. The lamellar regions are composed of continuous as well as discontinuous α_2 (ordered Ti_3Al phase with $D0_{19}$ crystal structure) lamellae in γ (ordered TiAl phase with $L1_0$ crystal structure) matrix. In addition, α_2/γ lamellar interfaces contain numerous nanometer-scale B2 (ordered Ti-based solid solution) and Ti_5Si_3 precipitates [31]. Fine B2 precipitates, formed at the α_2/γ interfaces before creep testing, improve the creep resistance of the alloy through hindering interface dislocation mobility, reducing generation of γ matrix dislocations from lamellae and preventing dislocations from passing through lamellar interfaces. In the case of the
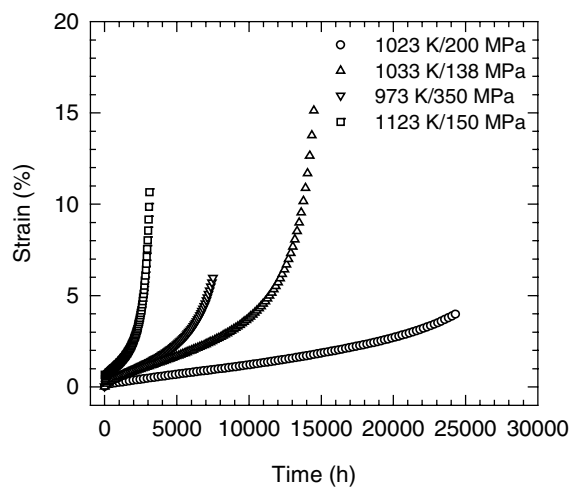
ABB-2 alloy, the strengthening effect of the B2 precipitates is enhanced by co-precipitation of fine Ti_5Si_3 particles along the lamellar interfaces with a similar effect on the dislocation mobility. The discontinuous α_2 lamellae contain fine needle-like particles with average width of 25 nm and length of 200 nm, which were identified to belong to B2-phase. Some lamellar regions contain large blocky type B2 particles with an average size of about 20 μm. These particles contain elongated particles, which belong to the γ-phase, and very fine Ti_5Si_3 precipitates [29]. The feathery regions are composed of the γ-phase, irregular α_2 lamellae, B2 particles and Ti_5Si_3 precipitates. The γ-rich regions are composed of the γ matrix and coarse spherical Ti_5Si_3 precipitates.

3.2. Creep

The creep deformation curves for the studied regimes are shown in Fig. 2. The creep curves exhibit short primary creep stage that is directly followed by the tertiary creep. Figure 3 shows the variation of instantaneous creep rate with the strain. During the primary creep stage the creep rate decreases with increasing strain. After reaching a minimum at a strain of about 1 %, the creep rate increases with increasing strain. No steady-state creep stage is observed over the studied temperatures from 973 to 1123 K and applied stresses ranging from 138 to 350 MPa. For rotating components like turbine blades, the maximum overall creep strain allowable for turbine blades depends on the engine tolerance but this strain usually should not exceed 1 % during the creep exposure up to 10000 h and 30000 h for the aircraft engines and stationary gas turbines, respectively. Table 2 summarizes the results of the creep tests including minimum creep rate and

time to 1 % creep deformation. It is clear that the time to 1 % creep deformation of 8100 h measured in the specimen tested at 1023 K is still shorter than that of 10000 h expected by the designers. Shorter time to 1 % deformation indicates that the applied stress of 200 MPa is too high and operating stress of turbine blade should be decreased to achieve creep strain limits.

Detailed analysis of creep deformation microstructures of the studied alloy at low creep strains (1–2 %) was published recently elsewhere [20, 22]. It was shown that the kinetics of creep deformation is controlled by non-conservative movement of ordinary dislocations in the γ matrix. The dislocations were elongated in the screw orientation and formed local cusps, which were frequently associated with the jogs on the screw segments of dislocations. Figure 4 shows the typical examples of deformation microstructures observed at higher creep strains. Besides the ordinary dislocations, local cusps and dislocation loops formed around the precipitates (Fig. 4a), the deformation microstructures of the studied creep specimen contain numerous deformation twins, as shown in Figs. 4b and 4c. As reported by Dlouhý et al. [21, 32], volume fraction of deformation twins increases with increasing creep strain. The formation of deformation twins contrib-
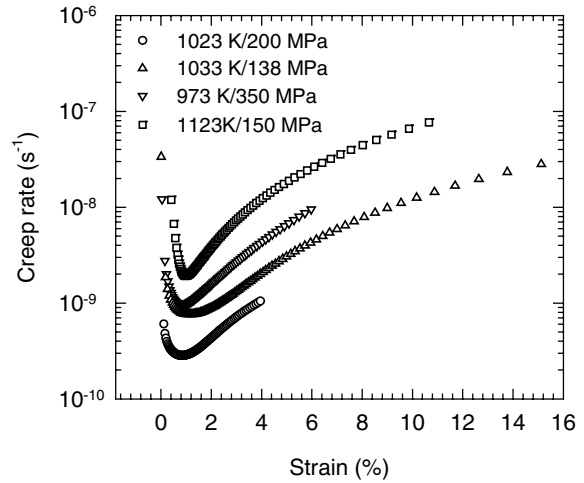

Fig. 3. Dependence of creep rate on the strain. The creep temperatures and applied stresses are indicated in the figure.

utes to an increase of creep rate during tertiary creep stage of pure and near γ-TiAl alloys. This contribution is twofold: (i) deformation twins relax incompatibility stresses during primary creep and (ii) supplies up to
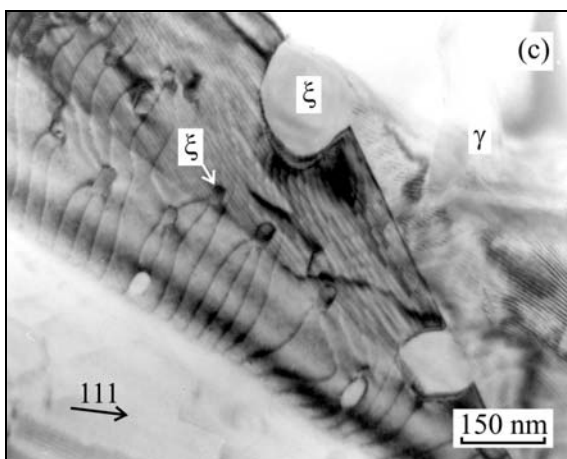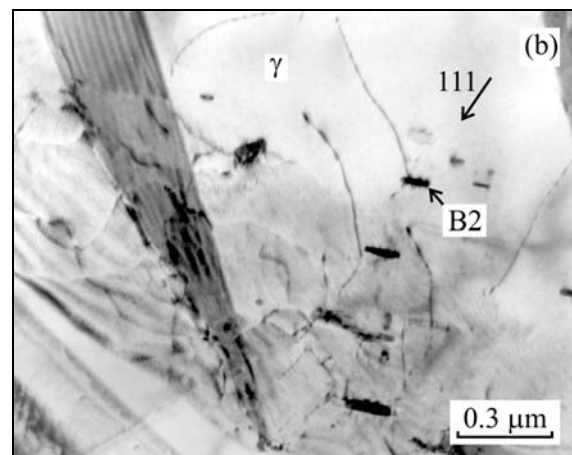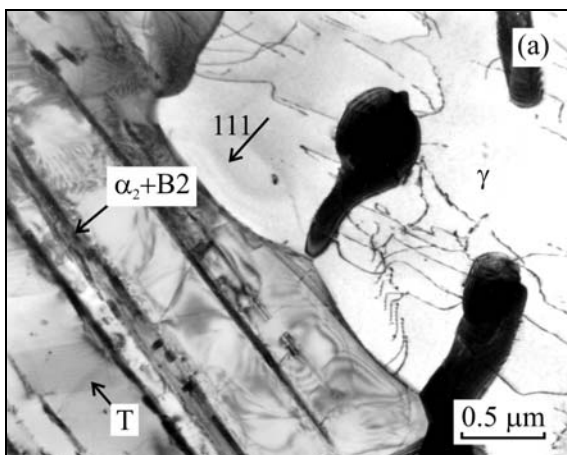

Fig. 4. TEM micrographs showing the typical deformation microstructure of the creep specimen tested at 1023 K/200 MPa to strain of 6.7 % for 25677 h: (a) ordinary dislocations formed in the γ matrix and deformation twins within γ lamellae (T); (b) deformation twins formed in the γ-rich region; (c) detail of deformation twin showing fine and coarser Ti_5Si_3 particles. Zone axis near $[1\bar{1}0]_\gamma$.
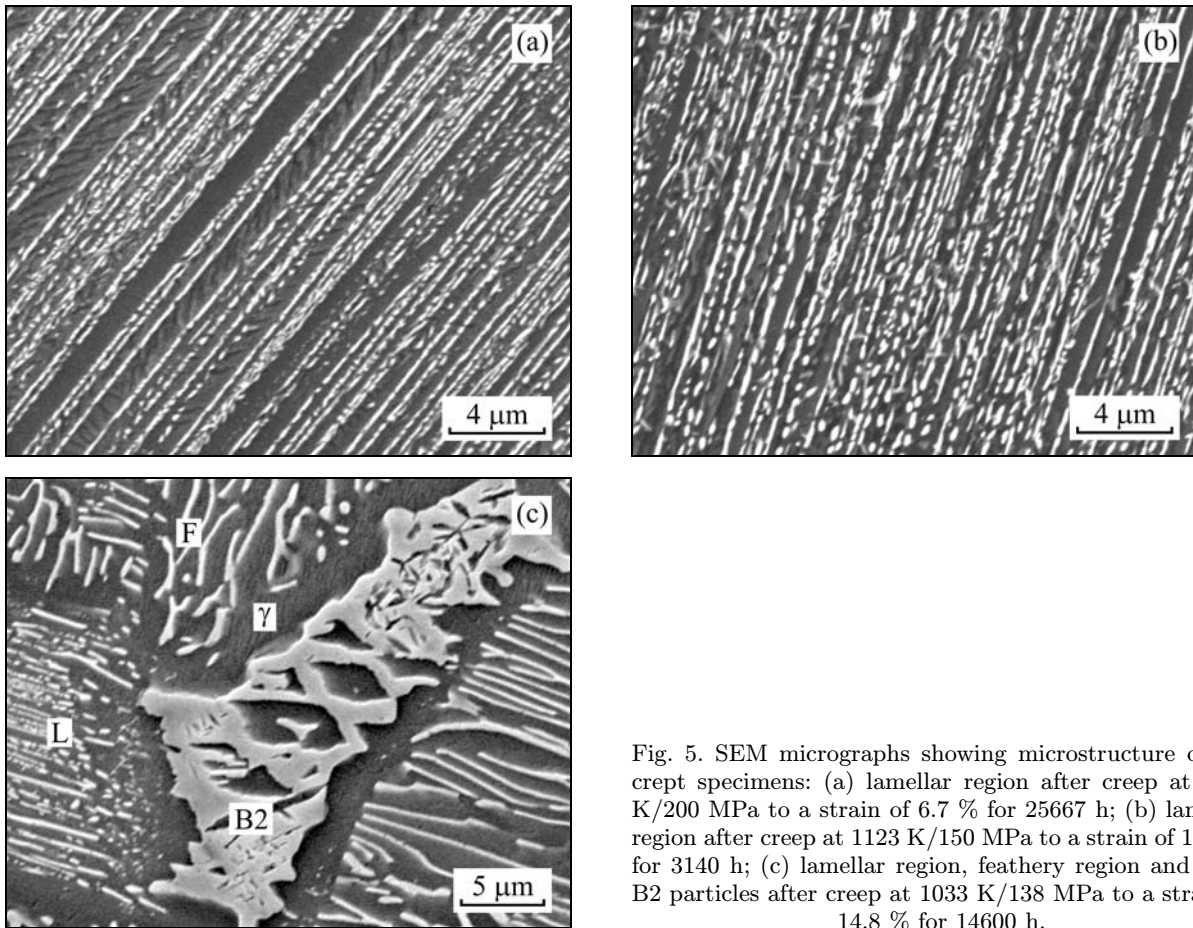
Fig. 5. SEM micrographs showing microstructure of the crept specimens: (a) lamellar region after creep at 1023 K/200 MPa to a strain of 6.7 % for 25667 h; (b) lamellar region after creep at 1123 K/150 MPa to a strain of 12.1 % for 3140 h; (c) lamellar region, feathery region and large B2 particles after creep at 1033 K/138 MPa to a strain of 14.8 % for 14600 h.
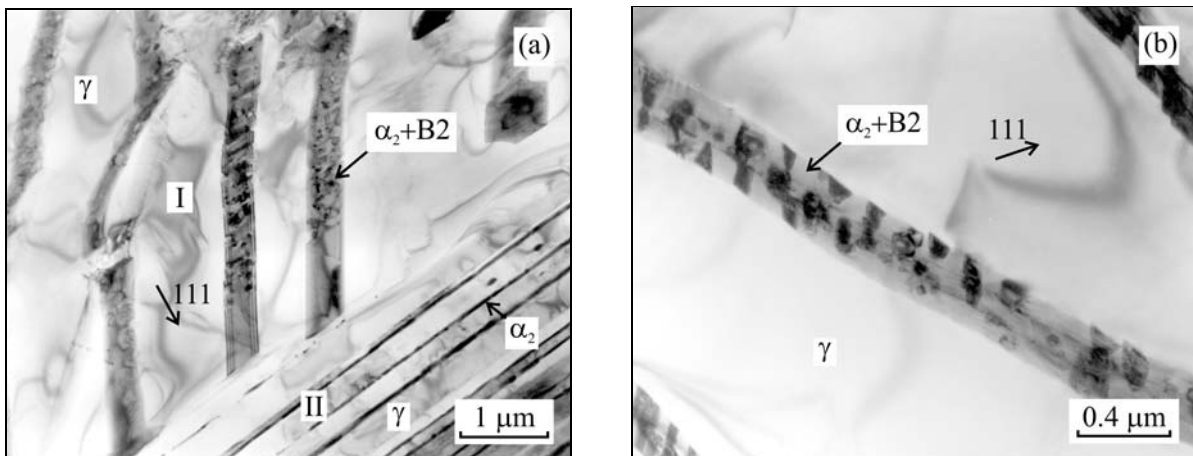

Fig. 6. TEM micrographs showing decomposition of the α_2 lamellae during creep at 1023 K/200 MPa to a strain of 6.7 % for 25677 h: (a) neighbouring grains with partially decomposed α_2 to the γ phase, B2 precipitates and Ti_5Si_3 silicides in the grain I and thin remaining α_2 lamellae and numerous γ lamellae in the grain II; (b) detail showing the decomposition of the α_2 lamellae. Zone axis near $[1\bar{1}0]_\gamma$.

30 % of the overall strain during tertiary creep stage. However, absence of steady-state creep stage during the creep of the multiphase ABB-2 alloy can be related not only to the formation of deformation twins but microstructural instabilities as well.

3.3. Microstructure stability during long-term creep testing

Figure 5 shows SEM micrographs illustrating the major changes occurring in the microstructure of the
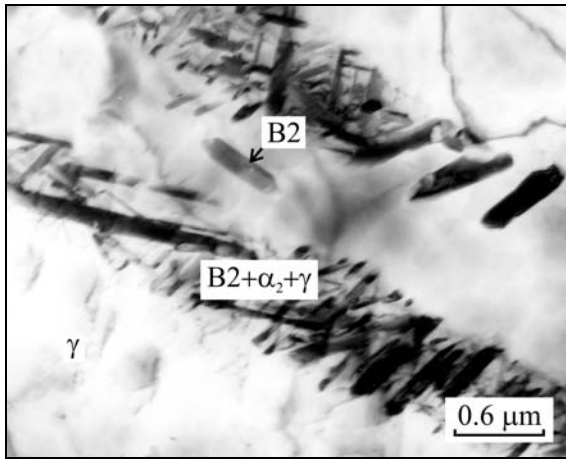
Fig. 7. TEM micrograph showing the transformation of the α_2 lamellae to needle-like B2 precipitates and γ phase in the feathery region during creep at 1033 K/138 MPa to a strain of 14.8 % for 14600 h.
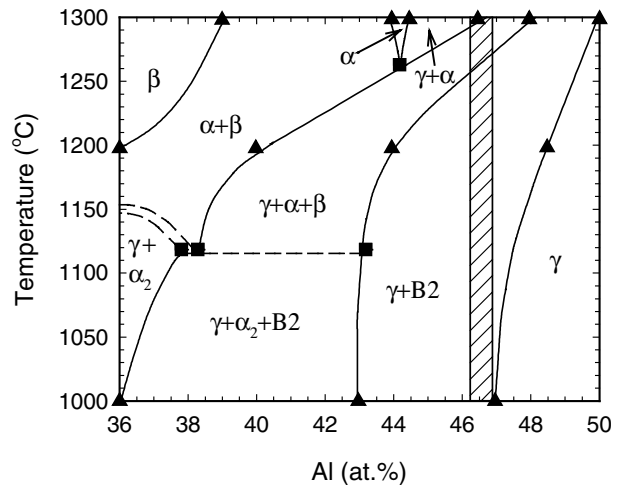

Fig. 8. Quasi-binary phase diagram for ternary Ti-Al-W with 2 at.% W according to Gil et al. [26]. The chemical composition of studied components is marked in the figure.

crept specimen. Figure 5a indicates partial dissolution of continuous α_2 lamellae, which transform to discontinuous segments at temperatures from 973 to 1033 K. Figure 5b illustrates early stages of globularization of the α_2 lamellae during the creep at the highest temperature of 1123 K. Full globularization of the α_2 phase in the lamellar regions of the ABB-2 alloy was reported by Muñoz-Morris et al. [26, 33, 34] during ageing at temperatures between 1223 and 1273 K. As seen in Fig. 5c, the creep exposure had no effect on the stability of coarse equiaxed B2 particles and apparently limited effect on the microstructure stability of feathery regions. However, detailed TEM observations revealed that the α_2 phase is unstable in both lamellar and feathery regions. Figure 6 shows decomposition of the α_2 phase during creep. As seen in Fig. 6a, fine elongated precipitates of B2 phase and equiaxed Ti_5Si_3 particles are formed within the α_2 lamellae in one of the grains (grain I). Figure 6b shows the detail of the B2 particles in the α_2 lamellae. The second grain (grain II) in Fig. 6a contains nearly fully decomposed thin α_2 lamellae and numerous γ lamellae. In some regions, the α_2 lamellae fully decomposed to needle-like B2 particles, as seen in Fig. 7. Quantitative metallographic analysis revealed that the applied stress accelerates coarsening kinetics of such needle-like B2 particles. While the ageing at 1023 K for 25677 h results in an increase of initial mean width of B2 precipitate from 25 to 75 nm and mean length from 200 to 590 nm, mean width of the precipitates was measured to be 95 nm and mean length was 805 nm in the gauge region of the creep specimen tested at 1023 K/200 MPa for the same time.

4. Discussion

It has been generally accepted that the best microstructure of TiAl-based alloys is a fine lamellar structure which provides the alloy with good creep resistance and fracture toughness. However, this lamellar structure should be sufficiently stable at operating conditions for a specific alloy. Previous works on the ABB-2 alloy showed that simple cast components can operate at 1023 K but this temperature should be decreased to 973 K for complex shaped large turbine blades due to lower creep resistance of their central parts [22, 24, 25]. As shown by Larson et al. [35], additions of tungsten stabilize α_2 lamellae against dissolution during ageing. In spite of adding tungsten to slow down diffusion kinetics in the ABB-2 alloy, the microstructure analysis clearly showed numerous microstructural instabilities connected with dissolution of the α_2 phase during high temperature exposure.

The main drawback of design of new TiAl-based alloys is the absence of reliable phase diagrams. In spite of the fact that several commercially available thermodynamic databases include data for calculation of phase composition of TiAl-based alloys, resulting phase diagrams are not reliable. Especially, addition elements, which slow down the diffusion kinetics, cannot be experimentally verified at assumed operating temperatures in reasonably short time. Figure 8 shows quasi-binary phase diagram suggested by Gil et al. [26], which was constructed from isothermal sections for the ternary Ti-Al-W alloys containing 2 at.% W alloys published by Kainuma et al. [36]. According to this phase diagram, the driving forces for microstructural changes in the ABB-2 alloy arise from changes of the phase equilibria. The $\gamma + \alpha_2 + $ B2 microstructure formed during thermal treatment is inherently

unstable and has tendency to transform to a stable γ + B2 during long-term creep testing. In spite of long-term creep tests, it was not possible to prove the validity of this quasi-binary phase diagram suggested by Gil et al. [26] for operating temperatures of about 973 K, which are of large interest for the industrial applications of the studied alloy. Since relatively large volume fraction of the α_2 phase was identified in each long-term crept specimen, we might still speculate that the phase diagram [26] is not valid and the final microstructure of ternary Ti-Al-W alloy should contain three $\gamma + \alpha_2$ + B2 phases instead of two γ + B2 ones.

The microstructural instabilities observed during creep are similar to those observed during long-term ageing of the ABB-2 alloy at the same ageing temperatures by Lapin et al. [30, 37, 38]. However, this process was very slow due to low diffusivity of tungsten. It was proved that the kinetics of the softening caused by these microstructural instabilities is very slow at assumed operating temperature of 973 K and cannot affect significantly mechanical properties of the turbine blades during their operating life up to 30000 h.

5. Conclusions

The investigation of the influence of long-term creep exposure on the microstructure stability of cast intermetallic Ti-46Al-2W-0.5Si (at.%) alloy for turbine blades suggests the following conclusions:

1. The creep deformation curves exhibit short primary creep stage that is directly followed by the tertiary creep. The minimum creep rate is found to depend on the applied stress and temperature and varies from 1.93×10^{-9} to 2.83×10^{-10} s^{-1} for the selected creep regimes.

2. The absence of secondary creep stage can be related to microstructural instabilities and formation of deformation twins. During creep testing the α_2 phase in the lamellar and feathery regions transforms to the γ phase, needle-like B2 precipitates and occasionally to fine spherical Ti$_5$Si$_3$ particles. The applied stresses are shown to accelerate coarsening kinetics of needle-like B2 precipitates.

3. Final microstructures of all crept specimens contain four phases $\alpha_2 + \gamma$ + B2 + Ti$_5$Si$_3$. In spite of long-term creep tests, it is not possible to prove the validity of the quasi-binary phase diagram suggested for ternary Ti-Al-W alloy with 2 at.% W at operating temperatures about 973 K, which predicts coexistence of two γ + B2 phases.

Acknowledgements

References

[1] LUKÁŠ, P.—ČADEK, J.—KUNZ, L.—SVOBODA, M.—KLUSÁK, J.: Kovove Mater., *43*, 2005, p. 5.

[2] ROGANTE, M.—ŠAROUN, J.—STRUNZ, P.—CESCHINI, G. F.—RYUKHTIN, V.—LUKÁŠ, P.—MARINČÁK, V.: Kovove Mater., *43*, 2005, p. 371.

[3] ZRNÍK, J.—SEMEŇAK, J.—HORŇAK, P.—VRCHOVINSKÝ, V.: Kovove Mater., *43*, 2005, p. 93.

[4] KUNZ, L.—LUKÁŠ, P.—MINTÁCH, R.—HRBÁČEK, K.: Kovove Mater., *44*, 2006, p. 275.

[5] LAPIN, J.—BAJANA, O.: Kovove Mater., *43*, 2005, p. 169.

[6] LAPIN, J.—MAREČEK, J.—KURSA, M.: Kovove Mater., *44*, 2006, p. 1.

[7] LAPIN, J.: Intermetallics, *14*, 2006, p. 1417.

[8] PRAHL, J.—HAUŠILD, P.—KARLÍK, M.—CRENN, J. F.: Kovove Mater., *43*, 2005, p. 134.

[9] KRATOCHVÍL, P.—SCHINDLER, I.—HANUS, P.: Kovove Mater., *44*, 2006, p. 321.

[10] KRATOCHVÍL, P.—MÁLEK, P.—PEŠIČKA, J.—HAKL, J.—VLASÁK, T.—HANUS, P.: Kovove Mater., *44*, 2006, p. 185.

[11] PRAHL, J.—HAUŠILD, P.—KARLÍK, M.—CRENN, J. F.: Kovove Mater., *44*, 2006, p. 134.

[12] VOJTĚCH, D.—ČÍŽOVÁ, H.—MAIXNER, J.: Kovove Mater., *43*, 2005, p. 317.

[13] LEYENS, C.—PETERS, M.: Titanium and Titanium Alloys – Fundamentals and Applications. Weinheim, Wiley-VCH Verlag GmbH & Co. KGaA 2005.

[14] NAZMY, M.—LUPINC, V.: In: Materials for Advanced Power Engineering 2002. Eds.: Lecomte-Beckers, J., Carton, J. M., Schubert, F., Ennis, P. J. Forschungszentrum Jülich GmbH, Vol. 21, Part I, 2002, p. 43.

[15] HARDING, R. A.: Kovove Mater., *42*, 2004, p. 225.

[16] SANIN, V.—YUKHVID, V.—SYTSCHEV, A.—ANDREEV, D.: Kovove Mater., *44*, 2006, p. 49.

[17] LAPIN, J.: Kovove Mater., *43*, 2005, p. 81.

[18] LAPIN, J.—GABALCOVÁ, Z.—BAJANA, O.—DALOZ, D.: Kovove Mater., *44*, 2006, p. 297.

[19] CHENG, T. T.—LORETTO, M. H.: Acta Mater., *46*, 1998, p. 4801.

[20] LAPIN, J.: Kovove Mater., *44*, 2006, p. 57.

[21] ORLOVÁ, A.—KUCHAŘOVÁ, K.—DLOUHÝ, A.: Kovove Mater., *43*, 2005, p. 55.

[22] LAPIN, J.: Intermetallics, *14*, 2006, p. 115.

[23] KISHIDA, K.—JOHNSON, D. R.—MASUDA, Y.—UMEDA, H.—INUI, H.—YAMAGUCHI, M.: Intermetallics, *6*, 1998, p. 679.

[24] LAPIN, J.—NAZMY, M.: Mater. Sci. Eng. A, *380*, 2004, p. 298.

[25] RECINA, V.—LUNDSTRÖM, D.—KARLSSON, B.: Metall. Mater. Trans., *33A*, 2002, p. 2869.

[26] GIL, I.—MUÑOZ-MORRIS, M. A.—MORRIS, D. G.: Intermetallics, *9*, 2001, p. 973.

[27] NAZMY, M.—STAUBLI, M.: U.S.Pat.#5,207,982 and European Pat.#45505 BI.

[28] LAPIN, J.—KLIMOVÁ, A.: Kovove Mater., *41*, 2003, p. 1.

[29] YU, R.—HE, L. L.—JIN, Z. X.—GUO, J. T.—YE, H. Q.—LUPINC, V.: Scripta Mater., *44*, 2001, p. 911.

[30] LAPIN, J.—PELACHOVÁ, T.: Kovove Mater., *42*, 2004, p. 143.

[31] YU, R.—HE, L. L.—CHENG, Z. Y.—ZHU, J.—YE, H. Q.: Intermetallics, *10*, 2002, p. 661.

[32] DLOUHÝ, A.—KUCHAŘOVÁ, K.—BŘEZINA, J.: Mater. Sci. Eng. A, *319–321*, 2001, p. 820.

[33] MUÑOZ-MORRIS, M. A.—FERNÁNDEZ, I. G.—MORRIS, D. G.: Scripta Mater., *46*, 2002, p. 617.

[34] MUÑOZ-MORRIS, M. A.—GIL, I.—MORRIS, D. G.: Intermetallics, *13*, 2005, p. 929.

[35] LARSON, D. J.—LIU, C. T.—MILLER, M. K.: Intermetallics, *5*, 1997, p. 497.

[36] KAINUMA, R.—FUJITA, Y.—MITSUI, H.—OHNUMA, I.—ISHIDA, K.: Intermetallics, *8*, 2000, p. 855.

[37] LAPIN, J.—PELACHOVÁ, T.: Intermetallics, *14*, 2006, p. 1175.

[38] LAPIN, J.—KLIMOVÁ, A.—PELACHOVÁ, T.: Scripta Mater., *49*, 2003, p. 681.